Research Article | Vol. 9, No. 1 | 1 Jan 2018 | BIOMEDICAL OPTICS EXPRESS 303
Biomedical Optics EXPRESS

Visualization of barriers and obstacles to molecular diffusion in live cells by spatial pair-cross-correlation in two dimensions

LEONEL MALACRIDA,[1,2,4] PER NIKLAS HEDDE,[1,4] SUMAN RANJIT,[1] FRANCESCO CARDARELLI,[3] AND ENRICO GRATTON[1,*]

[1]*Laboratory for Fluorescence Dynamics, Department of Biomedical Engineering, University of California, Irvine, USA*
[2]*Área de Investigación Respiratoria, Departamento de Fisiopatología, Hospital de Clínicas, Facultad de Medicina, Universidad de la República, Uruguay*
[3]*Center for Nanotechnology Innovation @NEST, Istituto Italiano di Tecnologia, Piazza San Silvestro 12, 56127 Pisa, Italy*
[4]*LM and PNH contributed equally to this work*
[*]*egratton22@gmail.com*

Abstract: Despite recent advances in optical super-resolution, we lack a method that can visualize the path followed by diffusing molecules in the cytoplasm or in the nucleus of cells. Fluorescence correlation spectroscopy (FCS) provides molecular dynamics at the single molecule level by averaging the behavior of many molecules over time at a single spot, thus achieving very good statistics but at only one point in the cell. Earlier image-based methods including raster-scan and spatiotemporal image correlation need spatial averaging over relatively large areas, thus compromising spatial resolution. Here, we use spatial pair-cross-correlation in two dimensions (2D-pCF) to obtain relatively high resolution images of molecular diffusion dynamics and transport in live cells. The 2D-pCF method measures the time for a particle to go from one location to another by cross-correlating the intensity fluctuations at specific points in an image. Hence, a visual map of the average path followed by molecules is created.

OCIS codes: (170.2520) Fluorescence microscopy; (110.2960) Image analysis; (110.4155) Multiframe image processing.

References and links

1. A. Kinkhabwala and P. I. Bastiaens, "Spatial aspects of intracellular information processing," Curr. Opin. Genet. Dev. **20**(1), 31–40 (2010).
2. J. E. Purvis and G. Lahav, "Encoding and Decoding Cellular Information through Signaling Dynamics," Cell **152**(5), 945–956 (2013).
3. C. Di Rienzo, E. Gratton, F. Beltram, and F. Cardarelli, "Fast spatiotemporal correlation spectroscopy to determine protein lateral diffusion laws in live cell membranes," Proc. Natl. Acad. Sci. U.S.A. **110**(30), 12307–12312 (2013).
4. C. Di Rienzo, V. Piazza, E. Gratton, F. Beltram, and F. Cardarelli, "Probing short-range protein Brownian motion in the cytoplasm of living cells," Nat. Commun. **5**, 5891 (2014).
5. E. Hinde, F. Cardarelli, M. A. Digman, and E. Gratton, "In vivo pair correlation analysis of EGFP intranuclear diffusion reveals DNA-dependent molecular flow," Proc. Natl. Acad. Sci. U.S.A. **107**(38), 16560–16565 (2010).
6. C. Eggeling, C. Ringemann, R. Medda, G. Schwarzmann, K. Sandhoff, S. Polyakova, V. N. Belov, B. Hein, C. von Middendorff, A. Schönle, and S. W. Hell, "Direct observation of the nanoscale dynamics of membrane lipids in a living cell," Nature **457**(7233), 1159–1162 (2009).
7. F. Cardarelli, L. Lanzano, and E. Gratton, "Capturing directed molecular motion in the nuclear pore complex of live cells," Proc. Natl. Acad. Sci. U.S.A. **109**(25), 9863–9868 (2012).
8. E. Hinde, F. Cardarelli, M. A. Digman, A. Kershner, J. Kimble, and E. Gratton, "The Impact of Mitotic versus Interphase Chromatin Architecture on the Molecular Flow of EGFP by Pair Correlation Analysis," Biophys. J. **100**(7), 1829–1836 (2011).
9. E. Hinde, F. Cardarelli, M. A. Digman, and E. Gratton, "Changes in Chromatin Compaction During the Cell Cycle Revealed by Micrometer-Scale Measurement of Molecular Flow in the Nucleus," Biophys. J. **102**(3), 691–697 (2012).

#307521 https://doi.org/10.1364/BOE.9.000303
Journal © 2018 Received 20 Sep 2017; revised 9 Dec 2017; accepted 11 Dec 2017; published 20 Dec 2017

Biomedical Optics EXPRESS

10. E. Hinde, K. Yokomori, K. Gaus, K. M. Hahn, and E. Gratton, "Fluctuation-based imaging of nuclear Rac1 activation by protein oligomerisation," Sci. Rep. **4**(1), 4219 (2015).
11. M. Baum, F. Erdel, M. Wachsmuth, and K. Rippe, "Retrieving the intracellular topology from multi-scale protein mobility mapping in living cells," Nat. Commun. **5**, 4494 (2014).
12. A. Honigmann, V. Mueller, H. Ta, A. Schoenle, E. Sezgin, S. W. Hell, and C. Eggeling, "Scanning STED-FCS reveals spatiotemporal heterogeneity of lipid interaction in the plasma membrane of living cells," Nat. Commun. **5**, 5412 (2014).
13. M. A. Digman and E. Gratton, "Imaging Barriers to Diffusion by Pair Correlation Functions," Biophys. J. **97**(2), 665–673 (2009).
14. E. Hinde, M. A. Digman, K. M. Hahn, and E. Gratton, "Millisecond spatiotemporal dynamics of FRET biosensors by the pair correlation function and the phasor approach to FLIM," Proc. Natl. Acad. Sci. U.S.A. **110**(1), 135–140 (2013).
15. E. Hinde, M. A. Digman, C. Welch, K. M. Hahn, and E. Gratton, "Millisecond Spatiotemporal Dynamics of FRET Biosensors by the Pair Correlation Function and the Phasor Approach to FLIM," Biophys. J. **102**(3), 198a–199a (2012).
16. F. Cardarelli, L. Lanzano, and E. Gratton, "Fluorescence correlation spectroscopy of intact nuclear pore complexes," Biophys. J. **101**(4), L27–L29 (2011).
17. S. Zhou, W. C. Lo, J. L. Suhalim, M. A. Digman, E. Gratton, Q. Nie, and A. D. Lander, "Free Extracellular Diffusion Creates the Dpp Morphogen Gradient of the Drosophila Wing Disc," Curr. Biol. **22**(8), 668–675 (2012).
18. P. Bianchini, F. Cardarelli, M. Di Luca, A. Diaspro, and R. Bizzarri, "Nanoscale Protein Diffusion by STED-Based Pair Correlation Analysis," PLoS One **9**(6), e99619 (2014).
19. C. Di Rienzo, E. Jacchetti, F. Cardarelli, R. Bizzarri, F. Beltram, and M. Cecchini, "Unveiling LOX-1 receptor interplay with nanotopography: mechanotransduction and atherosclerosis onset," Sci. Rep. **3**(1), 1141 (2013).
20. A. Honigmann, S. Sadeghi, J. Keller, S. W. Hell, C. Eggeling, and R. Vink, "A lipid bound actin meshwork organizes liquid phase separation in model membranes," eLife **3**, e01671 (2014).
21. D. R. Sisan, R. Arevalo, C. Graves, R. McAllister, and J. S. Urbach, "Spatially resolved fluorescence correlation spectroscopy using a spinning disk confocal microscope," Biophys. J. **91**(11), 4241–4252 (2006).
22. D. L. Kolin, D. Ronis, and P. W. Wiseman, "k-Space image correlation spectroscopy: A method for accurate transport measurements independent of fluorophore photophysics," Biophys. J. **91**(8), 3061–3075 (2006).
23. J. Ries and P. Schwille, "Studying slow membrane dynamics with continuous wave scanning fluorescence correlation spectroscopy," Biophys. J. **91**(5), 1915–1924 (2006).
24. J. W. D. Comeau, D. L. Kolin, and P. W. Wiseman, "Accurate measurements of protein interactions in cells via improved spatial image cross-correlation spectroscopy," Mol. Biosyst. **4**(6), 672–685 (2008).
25. M. Weiss, "Probing the interior of living cells with fluorescence correlation spectroscopy," Ann. N. Y. Acad. Sci. **1130**(1), 21–27 (2008).
26. N. Dross, C. Spriet, M. Zwerger, G. Müller, W. Waldeck, and J. Langowski, "Mapping eGFP Oligomer Mobility in Living Cell Nuclei," PLoS One **4**(4), e5041 (2009).
27. V. P. Chauhan, R. M. Lanning, B. Diop-Frimpong, W. Mok, E. B. Brown, T. P. Padera, Y. Boucher, and R. K. Jain, "Multiscale Measurements Distinguish Cellular and Interstitial Hindrances to Diffusion In Vivo," Biophys. J. **97**(1), 330–336 (2009).
28. D. J. Needleman, Y. Xu, and T. J. Mitchison, "Pin-Hole Array Correlation Imaging: Highly Parallel Fluorescence Correlation Spectroscopy," Biophys. J. **96**(12), 5050–5059 (2009).
29. J. Sankaran, M. Manna, L. Guo, R. Kraut, and T. Wohland, "Diffusion, Transport, and Cell Membrane Organization Investigated by Imaging Fluorescence Cross-Correlation Spectroscopy," Biophys. J. **97**(9), 2630–2639 (2009).
30. N. Gröner, J. Capoulade, C. Cremer, and M. Wachsmuth, "Measuring and imaging diffusion with multiple scan speed image correlation spectroscopy," Opt. Express **18**(20), 21225–21237 (2010).
31. T. Wohland, X. Shi, J. Sankaran, and E. H. K. Stelzer, "Single Plane Illumination Fluorescence Correlation Spectroscopy (SPIM-FCS) probes inhomogeneous three-dimensional environments," Opt. Express **18**(10), 10627–10641 (2010).
32. Z. Petrásek, J. Ries, and P. Schwille, "Scanning FCS for the Characterization of Protein Dynamics in Live Cells," Methods Enzymol. **472**, 317–343 (2010).
33. R. Berkovich, H. Wolfenson, S. Eisenberg, M. Ehrlich, M. Weiss, J. Klafter, Y. I. Henis, and M. Urbakh, "Accurate Quantification of Diffusion and Binding Kinetics of Non-integral Membrane Proteins by FRAP," Traffic **12**(11), 1648–1657 (2011).
34. J. Capoulade, M. Wachsmuth, L. Hufnagel, and M. Knop, "Quantitative fluorescence imaging of protein diffusion and interaction in living cells," Nat. Biotechnol. **29**(9), 835–839 (2011).
35. A. P. Singh, J. Krieger, A. Pernus, J. Langowski, and T. Wohland, "SPIM-FCCS: A Novel Technique to Quantitate Protein-Protein Interaction in Live Cells," Biophys. J. **104**(2), 61a (2013).
36. L. Potvin-Trottier, L. F. Chen, A. R. Horwitz, and P. W. Wiseman, "A nu-space for image correlation spectroscopy: characterization and application to measure protein transport in live cells," New J. Phys. **15**(8), 085006 (2013).
37. M. Guo, H. Gelman, and M. Gruebele, "Coupled Protein Diffusion and Folding in the Cell," PLoS One **9**(12), e113040 (2014).

Biomedical Optics EXPRESS

38. C. Di Rienzo, F. Cardarelli, M. Di Luca, F. Beltram, and E. Gratton, "Diffusion Tensor Analysis by Two-Dimensional Pair Correlation of Fluorescence Fluctuations in Cells," Biophys. J. **111**(4), 841–851 (2016).
39. J. Huisken, J. Swoger, F. Del Bene, J. Wittbrodt, and E. H. K. Stelzer, "Optical sectioning deep inside live embryos by selective plane illumination microscopy," Science **305**(5686), 1007–1009 (2004).
40. P. N. Hedde, M. Stakic, and E. Gratton, "Rapid Measurement of Molecular Transport and Interaction inside Living Cells Using Single Plane Illumination," Sci. Rep. **4**(1), 7048 (2015).
41. P. N. Hedde, L. Malacrida, S. Ahrar, A. Siryaporn, and E. Gratton, "sideSPIM - selective plane illumination based on a conventional inverted microscope," Biomed. Opt. Express **8**(9), 3918–3937 (2017).
42. P. D. Moens and L. A. Bagatolli, "Profilin binding to sub-micellar concentrations of phosphatidylinositol (4,5) bisphosphate and phosphatidylinositol (3,4,5) trisphosphate," Biochim. Biophys. Acta **1768**(3), 439–449 (2007).
43. D. Wüstner, L. M. Solanko, F. W. Lund, D. Sage, H. J. Schroll, and M. A. Lomholt, "Quantitative fluorescence loss in photobleaching for analysis of protein transport and aggregation," BMC Bioinformatics **13**(1), 296 (2012).

1. Introduction

Signal transduction at a sub-cellular level is a key element in the regulation of cell functions, cell fate and cell migration. In the compartmentalized environment of cells these transduction processes are regulated by a tight spatio-temporal control of molecular flow [1, 2]. The regulation of this molecular flow requires a complex interplay between the structure of the surrounding cellular components [3–5] and a spatio-temporal control of molecular-interactions [6, 7]. The consequence is a molecular transport that depends strictly on the molecular species, on the aggregations state, on the active state of the molecule and on the cell-cycle phase [8–12]. Despite the pivotal role of molecular flow coordination in the living cell, we lack systematic approaches to visualize the complex connectivity of the cell interior with high resolution and, at the same time, on the proper temporal scale. This lack of methods to visualize molecular connectivity is a significant limit for advancing our knowledge in signal transmission. Here, we developed algorithms based on the pair correlation approach to display 2-D molecular connectivity maps of the cell interior.

Molecular diffusion and transport processes are fundamental in physical, chemical and biological systems. Most of the methods proposed to measure diffusion in cells are based on fluorescence correlation spectroscopy (FCS) and provide only local information about the diffusivity of molecules in cells and tissues. Fluctuation-based techniques, FCS, STICS (Spatio-Temporal Image Correlation Spectroscopy) and RICS-(Raster-Scan Image Correlation Spectroscopy) are able to measure the diffusion coefficient at single pixels (FCS) or in a small region of a cell (STICS and RICS). Eventually, by measuring many points in sequence, FCS can produce a diffusion map of the cell interior; however, these approaches cannot measure the spatial communication between regions of the cell at the scale of an entire cell. Although local or average values are needed for estimating protein concentration and mobility, we cannot determine from these measurements the path followed by molecules after activation or upon interaction with molecular partners. Here we propose a method to detect molecular transport by measuring the cross-correlation of fluctuations for all the pairs of points in the sample. To this end, we expand the pCF (pair Correlation Function) concept [13] to 2-dimensional images (2D-pCF). The pCF function is defined by

$$pCF = G(\tau, r_0, r_1) = \frac{\langle F(t, r_0) \cdot F(t+\tau, r_1) \rangle}{\langle F(t, r_0) \cdot F(t, r_1) \rangle} - 1. \quad (1)$$

In Eq. (1), τ is the time delay between acquisitions of the fluorescence intensity, F, at two points, r_0 and r_1, in the image where the temporal average is indicated by the brackets. Briefly, when the (pair of) points are located further apart than two times the size of the point spread function, there is a maximum of the correlation function which appears at a time delay proportional to the average time a molecule takes to move between the two points. Publications from our lab using line scans described the basic principle of the pCF approach and demonstrated applications to determine molecular transport in cell compartments and

Biomedical Optics EXPRESS

among cell compartments [5, 8–10, 14, 15]. Using the pCF method along a line, we were able for the first time to describe the effect of chromatin on the flow of GFP in live cell nuclei [5, 8, 9]. We also measured fluxes between the cytoplasm and the nucleus and the delayed communication caused by the passage through the nuclear pore complex [7, 16]. Other successful applications of the pCF approach have been reported by other labs [11, 17–20]. However, all previous work was aimed at detecting the existence of correlated fluctuations between two distant points without constructing an image of all correlated points. If there is an obstacle in between the two points molecules will go around and it will take them longer to appear at the other location. Thus, 2D-pCF (Eq. (1)) detects barriers to diffusion and heterogeneity because the time of the correlation maximum is delayed in the presence of diffusion barriers. In a nutshell, this non-invasive, sensitive technique can follow the same molecule over a large area producing a map of molecular diffusion. It does not require isolated molecules; thereby, many molecules can be labeled with the same fluorophore and be within the same volume of excitation (the PSF).

The 2D-pCF approach is a change of paradigm from both a technological and a conceptual point of view. From the technological perspective we need very high resolution spatial sampling coupled with a large field of view, and very high time resolution coupled with high sensitivity detection in order to measure the fluctuations due to fast moving and dim molecules in a whole cell. Currently, this can be achieved using fast and highly sensitive cameras. Then, from a conceptual point of view, we need an efficient algorithm able to visualize the connectivity between ~10^5-10^6 points in one slice of the cell interior, i.e., cross-correlate the fluctuations between all pairs of points of large images collected for a certain period of time. Although many investigations have focused on the study of the dynamical properties of proteins in live cells, most of the results are local, purely temporal or spatially averaged and in all these cases spatial communication is not visualized [11, 21–37]. Also, many of the current approaches require an interpretative model and a consequent analytical relationship between the measured properties (usually a change in fluorescence intensity) and the physical properties of the particle motion (e.g., diffusion coefficient). In order to unveil something unknown, such as the spatial communication in the cell, a model-free approach is required.

In this article we show that average molecular trajectories can be measured by the 2D-pCF approach without specific single molecule localization algorithms as used in single particle tracking. The experimental proof of these concepts shows that the 2D-pCF can be applied in live cells using available fluorescent chimeras of functional proteins and thus utilizes common techniques for protein labeling and expands our ability to quantify key players in cellular flow. Furthermore, the practical demonstration of connectivity maps may result in a breakthrough in the study of biochemical communication in live cells, by unveiling the role of the cell spatial organization in signal spreading, as well as describing the route followed by the signal molecules to spread from the source to the target.

2. Identifying barriers to diffusion by the 2D-pCF approach

In a spatially heterogeneous environment, the local diffusion coefficient is not sufficient to accurately describe the transport of molecules to neighboring regions. Penetrable or impenetrable barriers can shape the trajectories of molecules, guiding and confining molecular diffusion.

Biomedical Optics EXPRESS

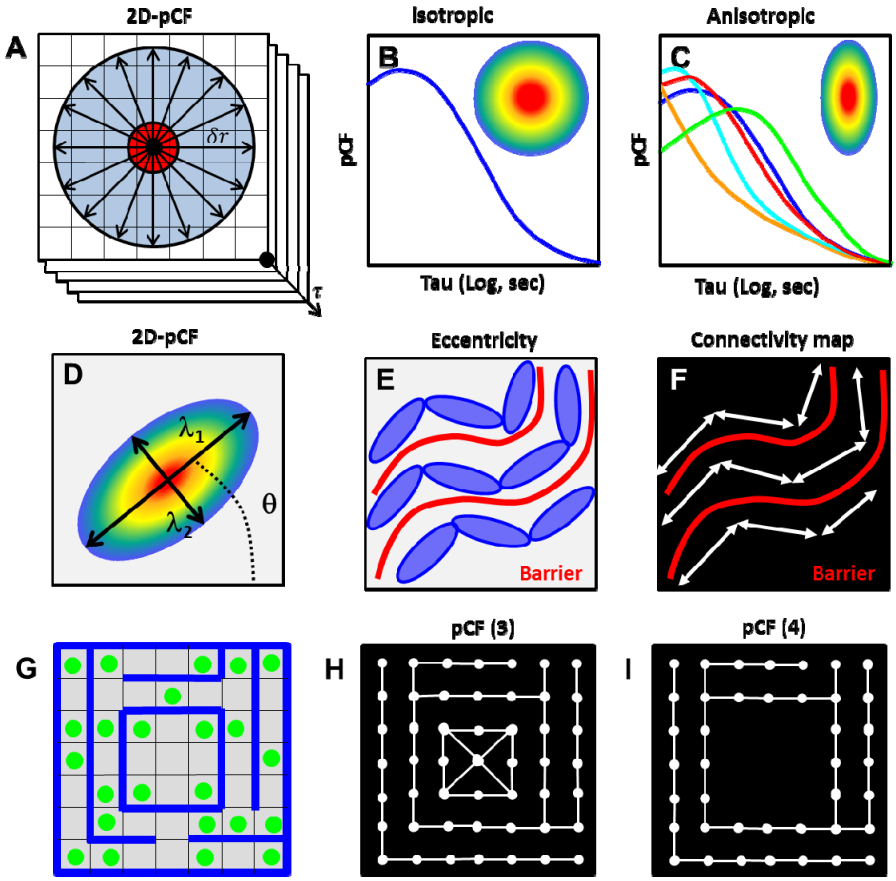

Fig. 1. Pictorial representation of the principle of the 2D-pCF to detect molecular transport in cells guided by obstacles and molecular interactions. A) Camera image time stack of the same focal plane (5,000 to 50,000 images) giving access to a grid of points where fluctuations due to the underlying molecular flow can be measured. B) The 2D-pCF is computed between every pair of points of the image and at a given distance. In an isotropic environment. Starting from a point, all the correlation functions should be equal and independent of the direction. The pCF correlation functions can have a maximum. C) If the environment is anisotropic, molecules could take longer to reach a given distance depending on the direction. D) The polar image resulting from plotting all the correlation functions as a function of the angle (2D-pCF) is analyzed using the first and second central moment (Eqs. (2)-(7)). E) The 2D-pCF is plotted using only the long axis of the ellipses shown in D. The definition of the axes lengths is given in Eq. (5). F) By joining the segments corresponding to the long axis we obtain the connectivity map that delineates the presence of barriers shown in red. G) If an underlying structure is present, shown schematically by a maze, the spatial connectivity can be obtained using different radii for the calculation of the 2D-pCF. H) The 2D-pCF function at a distance of 3 pixels for this maze reveals connected points at a small scale. I) The 2D-pCF calculated at a larger distance (4 pixels) show paths connected at a larger scale in the maze, and where there is an obstacle (center of the maze). The distance for the calculation of the 2D-pCF is used to reveal different barriers.

As shown in Fig. 1(A), we start with a stack of images of the same focal plane in the cell. From this stack we isolate a point and then we produce a set of correlation functions 2D-pCF(δr) at a given distance, δr, at different angles around a given point. This set for one particular distance δr can be plotted in a polar plot as a heat map where the hotter colors indicate larger values of the 2D-pCF function (Fig. 1(B)). We used a log scale for the delay time variable (Fig. 1(B)), as this is common practice in FCS. Note that the 2D-pCF is calculated at a given distance which can be varied producing visualizations of the 2D-pCF

Biomedical Optics EXPRESS

that show the path of molecules that travel long distances. For example, if there is an obstacle at a given distance from the original point r_0, for shorter distance we could observe changes of the correlation function at given angles that indicate the presence and local direction of the obstacle. But if we look at a longer distance we could observe that a particle has reached a distant position at much later times going around the obstacle (Fig. 1(G)-1(I)).

Figure 2 shows 2D-pCFs calculated at specific points in the image and the algorithm for the calculation of parameters sufficient to describe the lack of symmetry of the 2D-pCF (Fig. 2(J)).

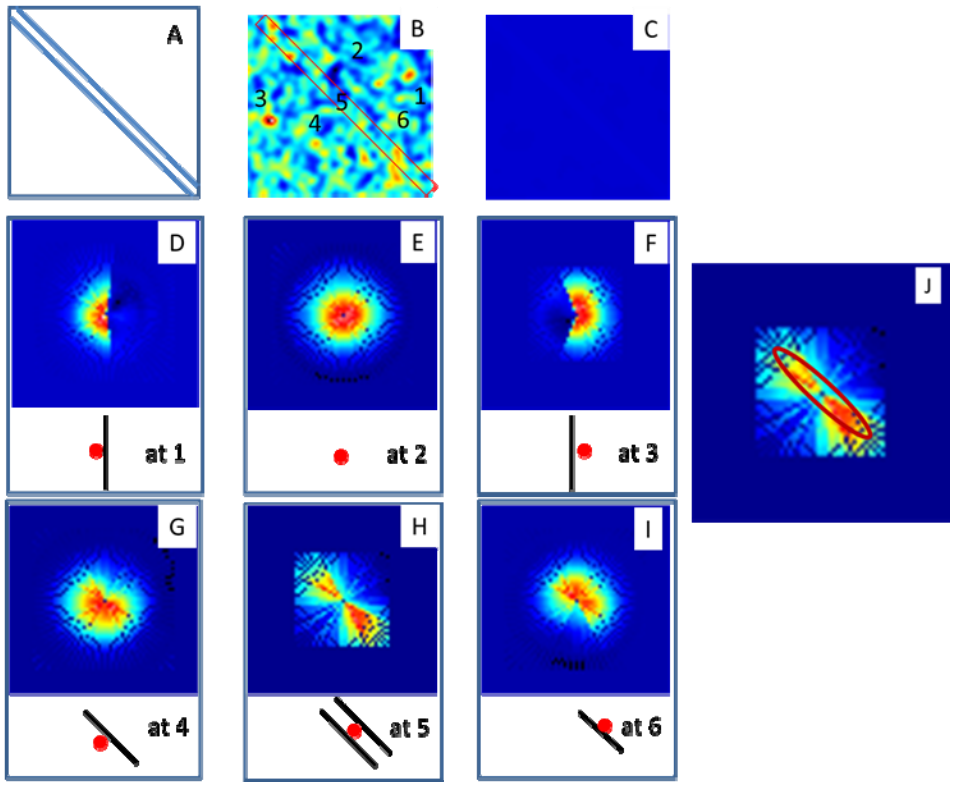

Fig. 2. Simulated experiment of diffusion in disconnected regions crossed by a narrow channel. A) A channel (300 nm wide) with impenetrable walls where molecules can diffuse surrounded by two regions which are mutually disconnected. The 2D-pCF is calculated according to Eq. (1) using 32 angles at a distance of 4 pixels. B) Intensity of a single image. C) Average intensity of all images D) 2D-pCF at one pixel from the right border of the image at point 1. E) 2D-pCF in a region far from the borders at point 2. F) 2D-pCF at 2 pixels from the left border at point 3. G) 2D-pCF at 2 pixels below the channel, point 4. H) 2D-pCF in the channel at point 5. I) 2D-pCF at 1 pixel above the channel, point 6. The presence of the discontinuity due to the channel can be seen in panels G, H and I although the walls of the channel are invisible since they are not labeled. J) Computed analysis of the shape of the 2D-pCF according to Eqs. (2)-(7) using the pattern of panel H. For this simulation the PSF was 300 nm, the pixel size was 114 nm and the total field of view was 7.2 μm. The image has 64x64 pixels and 32,768 images were simulated; the particle density for this simulation was 10 molecules/μm^2, which is a low value compared to experimental situations. Note that the 2D-pCF gives different patterns by moving the center of the calculation by one pixel as shown in panels D and F. Panels D-J show an image representing the 2D-pCF in a polar plot. The axes are in log-delay time. The maximum delay time is equal to 164s.

In Fig. 2 we show pCF polar maps for a simulated situation. We use image processing methods to obtain parameters of the angular distribution of the pCF. For this article, we use the first and second central moments of the spatial distribution; higher moments are ignored.

Biomedical Optics EXPRESS

For each point and for each distance we describe the angular distribution using few parameters (Fig. 2(J) and Eqs. (2)-(7)).

$$M_{ij} = \sum_x \frac{\sum_y x^i y^j I(x,y)}{\sum_x \sum_y I(x,y)} \tag{2}$$

$$\mu_{pq} = \sum_x \sum_y \left(x - \bar{x}\right)^p \left(y - \bar{y}\right)^q I(x,y) \tag{3}$$

$$\theta = \frac{1}{2} \arctan\left(\frac{2\mu_{11}}{\mu_{20} - \mu_{02}}\right) \tag{4}$$

$$\lambda_i = \frac{\mu_{20} + \mu_{02}}{2} \pm \frac{\sqrt{4\mu_{11}^2 + \left(\mu_{20} - \mu_{02}\right)^2}}{2} \tag{5}$$

$$Eccentricity = \sqrt{1 - \frac{\lambda_2}{\lambda_1}} \tag{6}$$

$$Anisotropy = \frac{\lambda_1 - \lambda_2}{\lambda_1 + \lambda_2} \tag{7}$$

I(x,y) in Eq. (2) is the value of the 2D-pCF correlation function at pixels shifts *x* and *y*. M_{ij} is the definition of the moments of the distribution of the 2D-pCF. The shift of the center of mass of the distribution (the μ parameters at the first order) can be used to obtain the net velocity of the particle if the evaluation of the pCF is done at multiple distances. From Eq. (3), the displacement of the center of mass is expressed in the unit of pixels of the image. In Eq. (5), the values of the parameters λ correspond to the long (λ_1) and short (λ_2) axis of the ellipses shown schematically in Fig. 2(J). In Eq. (5) the units of the length of the ellipses axes (second order moments) are in pixels square and they indicate how much the pCF distribution expands. As previously discussed [5], the pCF is larger and the peak of the pCF will appear at shorter time for faster diffusion. Using this principle, the difference between the long axis and the short axis of the ellipses indicate that in the direction of the long axis the pCF distribution is expanding faster. In this work, we use the long and short axis of the ellipses only as an indication of the extent of the anisotropy of the diffusion and of the direction of the preferential anisotropy. For this reason we use the ratio (or normalized difference) of the long and short axis of the ellipses to construct a map indicating where the pCF distribution is expanding anisotropically. To summarize, the second order moments are analyzed in terms of the anisotropy or eccentricity of the angular distribution (Eqs. (6) and (7)) which are related to the size of the major and minor axis of the ellipses describing the second moment distribution and the angle of the major axis of the ellipses (Eq. (4)) that indicates the local direction of the diffusional motion. The analysis software provides six maps, the intensity at each point, the values of the long and short axis of the ellipses and the angle of the ellipses, the values of the displacement of the center of mass and the average value of the pCF. The long and short axes of the ellipses are used to calculate the eccentricity (or anisotropy) of the diffusion, the two components of the position of the center of mass are used to calculate the direction and the modulus of the displacement of the center of mass of the pCF distribution.

Along each line as a function of the angle, if we change the distance, the time of the maximum of the pCF correlation function could be related to the mean square displacement (MSD) since the pCF represents the time it takes for a particle to reach a certain distance (Fig. 4). From the MSD we could obtain local diffusion coefficients and other parameters such as local confinement or the coefficient of anomalous diffusion. This calculation is not used in

Biomedical Optics EXPRESS

this article since the derivation of the diffusion coefficient form the slope of the MSD plot as a function of time delay assumes that the motion is isotropic, which is not the case for the data on cells used in this work. The calculation of the diffusion tensor has recently been presented and we are not repeating here the major findings of that paper [38]. Instead, we will discuss here how to obtain high resolution connectivity maps of the cell interior. The analysis using the moments of the distribution of the radial 2D-pCF function shown in Fig. 2(J) can be used as the set of rules for the classification of the molecular movement in different parts of an image to produce a map of obstacles and a map of the regions where the space is connected.

3. Simulations of molecules diffusing in a plane with a 300 nm channel

Figure 3 shows the analysis of the channel simulation used in Fig. 2 in which molecules are free to diffuse in a plane in which there is a 300-nm wide channel that simulates the presence of guided diffusion. We applied the 2D-pCF algorithms described in the discussion of Fig. 2 and in Appendix at each pixel of the simulation shown in Fig. 3. The intensity is relatively uniform since the particle density was about the same in the region of simulation (64x64 pixels) as shown in Fig. 3(A). The calculation of the eccentricity (Eq. (6)) is done by first calculating the central moments of the radial 2D-pCF function. For this figure the calculation was done at four pixels distance. The eccentricity is plotted as a heat map on a scale of 0 to 1, where 1 corresponds to the hottest color. For the connectivity map the threshold for the eccentricity was set at 0.45 (Fig. 3(D)). Only points close to the channel or inside the channel have larger eccentricity than the threshold value. For these points a segment of 10 pixels length is drawn in the direction of the ellipses as described in the Appendix. Figure 3(B) shows that only pixels near the channel wall or inside the channel display anisotropic diffusion. Note that the motion of particles is highly anisotropic in the channel and in the proximity of the channel. Only points with an eccentricity larger than 0.3 are plotted but Fig. 3(B) shows that there is a region outside the cannel where the motion has different degrees of eccentricity. This is because in Eq. (5), by definition, the values of the long axis λ_1 are always greater than the values of the short axis λ_2. A value of 0.45 was obtained in the case of random motion in the absence of obstacles/barriers and used as lower threshold for regions of random motion for data visualization. In Fig. 4(A) we show the eccentricity histogram obtained for a solution of EGFP where we should have only isotropic motion. The eccentricity histogram of all pixels of the map has a maximum around 0.45 which matches the result from the simulations.

Biomedical Optics EXPRESS

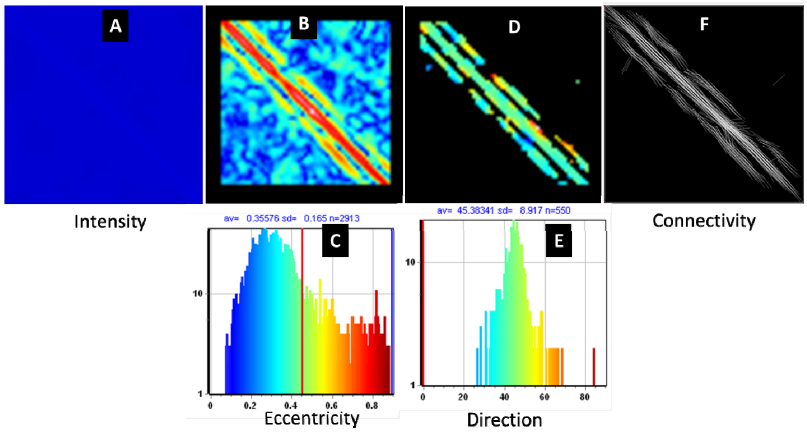

Fig. 3. Simulation of molecules diffusing in a plane with a 300 nm wide channel along the diagonal. For this simulation the pixel size was 114 nm and 32,768 frames were simulated. The molecules have a diffusion coefficient of 1 $\mu m^2/s$ and the frame rate was 100 frames/s. A) Average intensity of the 32,768 frames. The channel is invisible in the intensity image since the molecular density is uniform. B) Eccentricity map obtained using the algorithms of the analysis of the shape of the 2D-pCF. C) the histogram of the eccentricity values obtained for all pixels in the image. D) The direction of the major axis of the eccentricity polar plot, E) The histogram of the direction for all pixels with eccentricity above the threshold value marked by the red vertical line in C). The angle is in degrees and the scale is red to blue (horizontal-vertical. F) Connectivity map obtained by drawing segments in the direction given by the direction map and length proportional to the eccentricity values. Only segments with eccentricities larger than the threshold value are shown. The black regions in panel D and F correspond to isotropic diffusion. The color of the eccentricity and angle map is the same color used for the histogram values.

Figure 3(F) shows the connectivity map for points above the threshold of 0.45 for the eccentricity. Regions of connected diffusional flow are in the channel and around the channel (few regions). The channel is not labeled with any marker yet the connectivity map can visualize the channel. Black regions in Fig. 3(F) correspond to regions of isotropic motion.

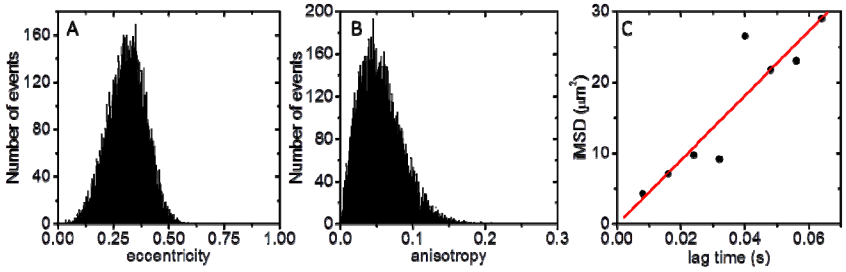

Fig. 4. 2D pCF and iMSD analysis of a 10 nM EGFP solution. A total of 8,192 frames (128 x 128 pixels) were acquired at a rate of 125 frames/s using selective plane illumination as described in the Appendix with 488 nm light (1 mW). A) Histogram of the eccentricity values; the average eccentricity was 0.31 ± 0.08 (mean ± SD). B) From the same data, the anisotropy was calculated according to the equations Eqs. (2-7) in the manuscript. The histogram is shown in the middle panel (0.06 ± 0.03). This shows that, even in the absence of barriers, obstacles or directed motion, we get an eccentricity value >0. This is because in Eq. (5) the values of λ_1 is always greater than λ_2. This value of 0.3 obtained in the case of random motion in the absence of barriers was used as lower threshold for regions of random motion for data visualization. C) To demonstrate that the fluorescence fluctuations were caused by free diffusion of EGFP in solution, the iMSD of the same data was calculated as shown on the right hand side, the resulting diffusion coefficient was 114 $\mu m^2/s$, which is in within the range of values found for EGFP in solution. This example shows that the data used for the 2D-pCF could also be used far from obstacles to measure the diffusion coefficient.

Biomedical Optics EXPRESS

In Fig. 5 we show a simulation of particles moving in and around a relatively small square box. The side of the box is 16 pixels which in the simulation (a pixel is 50 nm) correspond to a size of 0.8 μm, comparable to structures found in the cell nucleus or large vesicles. Figure 5 shows that the connectivity pattern caused by a small box has lines that depart from the surface. This is due to the high curvature of the structure simulated. This simulation shows that the simple rules used to explain the eccentricity patterns illustrated in Fig. 2 are valid for borders of low curvature but for highly curved structures additional rules must be considered. The pattern is fully reproducible in the simulation. This is not a random speckle but it is what is expected for the diffusion anisotropy close to corners and at points of high curvature. In principle, we can simulate any structure in both 2D and 3D that will help to recognize the observed patterns. The pattern simulated in Fig. 5 will be discussed later in conjunction with patterns of connectivity found in live cells.

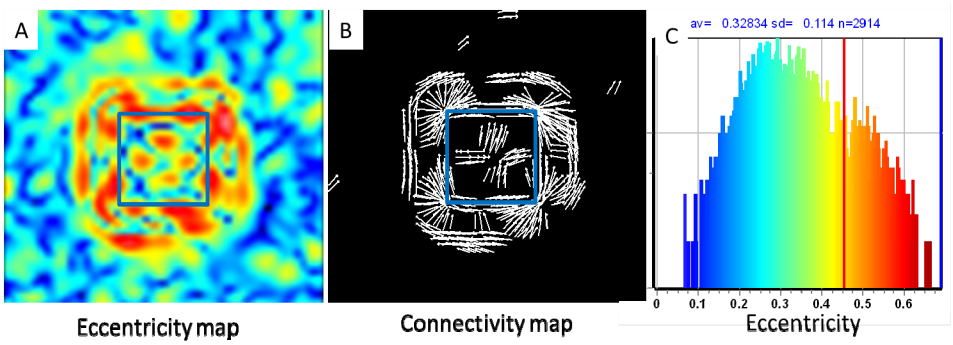

Fig. 5. Simulation of molecules moving in a plane where there is an impenetrable box. The size of the box is 0.8 μm x 0.8 μm, comparable to structures found in the cell nucleus and large vesicles. The particle density for this simulation is 8.7 molecules/μm^2. Local diffusion coefficient is 10 μm^2/s both inside and outside the box. The box is impenetrable. The 2D-pCF was calculated for a distance of 4 pixels. In the simulation the waist of the PSF was 200 nm. The camera frame rate was set to 100 frames/s and a total of 16,384 frames were analyzed. A) The eccentricity map obtained using the algorithms in the manuscript. The noise is due to the low particle density. B) Connectivity map using a threshold of 0.45 for the eccentricity values to be included in the connectivity map. Note that in this structure and at regions of high curvature there are connectivity lines perpendicular to the box side in addition to connectivity lines parallel to the box sides. C) Eccentricity histogram color coded using the same colors in the eccentricity map.

4. Experimental validation of the 2D-pCF method

4.1 EGFP molecules moving in artificial grooves

In order to measure the fluctuations on a grid of points, the first requirement is fast frame acquisition of at least one optical section of the 3D intracellular space. By the classical raster-scan confocal approach the acquisition time increases linearly with the number of pixel measured and thus the sampling time required to measure the transport of small molecules (in the ms range) can only be achieved using a very fast frame rate scanner or in one dimension (a line scan). If the sample is inherently flat (<1 μm), there is no need for optical sectioning and a standard epifluorescence illumination with fast, camera-based image acquisition is adequate. As a first experimental verification of the 2D-pCF method for 2D diffusion we prepared a surface with periodic grooves 450 nm deep and 450 nm wide by stamping this pattern into a thin layer of PMMA on top of a glass cover slip. An electron microscopy image of the resulting pattern is shown in Fig. 6(A). To close the channels, a second cover slip was pressed on top of the grooves. Subsequently, the channels were filled with a 30 nM solution of monomeric EGFP and the sample was subjected to epifluorescence imaging with a camera frame rate of 100 Hz. Clearly, the channels exhibit a higher fluorescence intensity indicated

Biomedical Optics EXPRESS

by hotter colors in Fig. 6(B). Application of the 2D-pCF algorithm to the image time series yield the eccentricity map shown in Fig. 6(C). All channels show the same directionality indicating guided diffusion as we expected from this pattern. The direction of the molecular flow along the channels was visualized plotting the connectivity map (Fig. 6(D)) as described in the Appendix.

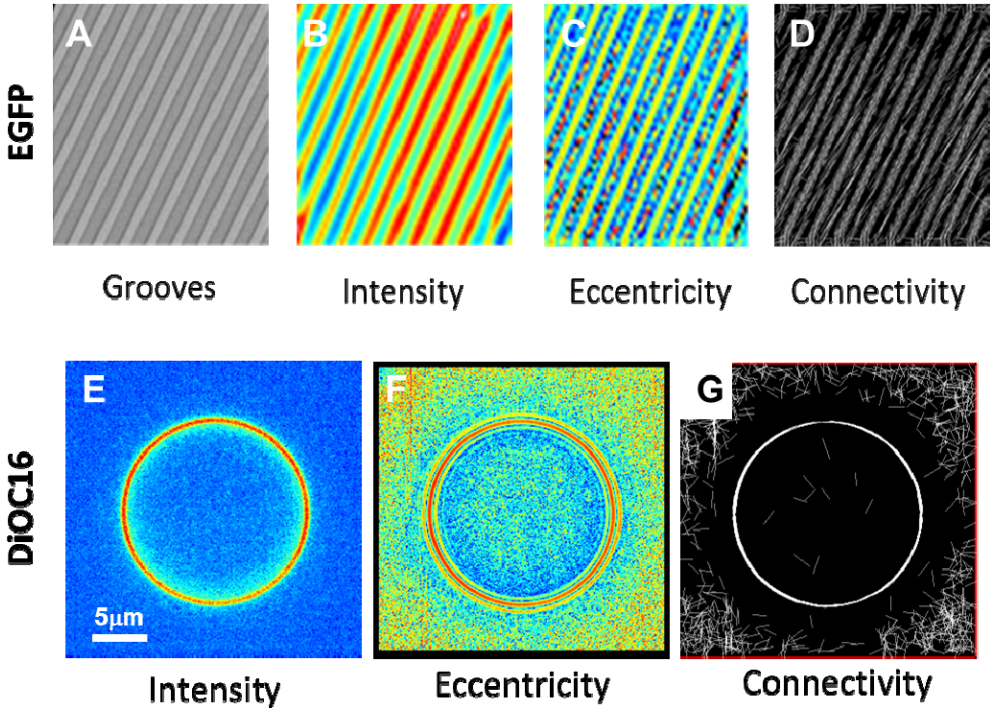

Fig. 6. Measuring the connectivity maps in testing samples. A 30 nM solution of EGFP is spread on top of a slide with grooves 450 nm deep and 450 nm wide. A cover glass is on top of the sample to maintain the solution in the grooves. The image was acquired in a wide field microscope equipped with an EMCCD camera at 100 frames/s; a total of 10,000 frames was collected for a total time of 100 s. The 2D-pCF algorithms were used to calculate the eccentricity and the connectivity maps. A) EM images of the grooves. B) The grooves containing a 30 nM EGFP solution. C) Eccentricity map. D) Connectivity map. EGFP molecules only diffuse in the groove as shown by the connectivity map. E) Intensity image of a GUV membrane labeled with DiOC16 in the sideSPIM microscope equipped with a sCMOS camera. F) Eccentricity map. G) Connectivity map. For the connectivity maps the eccentricity threshold was 0.45.

4.2 Visualizing the connectivity map in biological samples

In order to apply the 2D-pCF method to biological samples, we will take advantage of the widefield and SPIM microscope methods available in many laboratories today. For example, the SPIM microscope uses a low NA objective to produce a single plane of excitation light in the sample and a second (high NA) objective perpendicular to the first to collect the fluorescence light produced in the sample (see Figs. 8(A), 8(B)). By measuring the emission with a camera, the frame acquisition time in this microscope configuration can be pushed to the millisecond range. In the classical SPIM setup, the light sheet was obtained by placing a cylindrical lens in the excitation light path [39]; in the SPIM we built in our lab instead, the light sheet is obtained by rapid scanning of a focalized cone of light. This detail in the design of the microscope holds several advantages. For the purpose of this paper it is important that we can control the width of the light sheet by limiting the scan range. Moreover, the real

Biomedical Optics EXPRESS

exposure time of the sample can be controlled independently from the camera readout, avoiding the blurring effect caused both by particle motion during the exposure time and charge transfer during camera readout in rolling shutter mode. In fact, both EMCCD and sCMOS based detector arrays apply readout protocols that are "shutter free" in order to improve the read out speed. In other words, during shifting of charges produced by the incoming light in the sensor, the sensor is still exposed to light. Thus, a continuous exposure will introduce a trail in the image. Moreover, particularly in the case of an EMCCD camera, in order to decrease the acquisition time below 1 ms in the readout protocol, the photoelectrons are dynamically stored in a region of the chip that is outside the region of interest (ROI) but exposed to the incoming light. In order to avoid image overlapping, the chip outside the ROI has to be covered. Using a scanned beam, we can simply limit the size of the light sheet. The overall performance of our setup for detecting fast molecular dynamics in live cells has been already demonstrated in a recent publication [40].

4.3 Diffusion of DiOC16 in a GUV measured with the sideSPIM microscope

So far, we have shown connectivity maps for measurements done for simulated molecules moving in a channel and EGFP molecules diffusing in physical grooves where we had a clear expectation of the path followed by the molecules. In both cases the measured connectivity map was consistent with the expected pattern. Another model system where we can easily predict the direction of the diffusion are giant unilamellar vesicles (GUVs). We prepared GUVs labeled with dye molecules that are diffusing in the membrane so that the connectivity should only occur in the membrane itself (Figs. 6(E)-(G)). Figure 6(G) shows that, indeed, there is connectivity only along the membrane bilayer. The data for the GUVs experiments were collected with the sideSPIM microscope [41].

5. Application of the 2D-pCF method to visualize barriers to diffusion in live cells

5.1 U2OS cells labeled with DiOC18 measured on a widefield microscope using epi-illumination

In this measurement, the dye is labeling all membranes of the cell as shown in Fig. 7(A). The eccentricity map (Fig. 7(B)) shows strong anisotropic motion associated with membrane features and the connectivity map (Figs. 7(C), 7(D)) shows that the diffusive pattern is mainly along the membrane features. Note that each membrane seems to show two regions of anisotropic diffusion similarly to what was obtained in the simulations of diffusing molecules in the presence of a channel (Fig. 7(C)).

Biomedical Optics EXPRESS

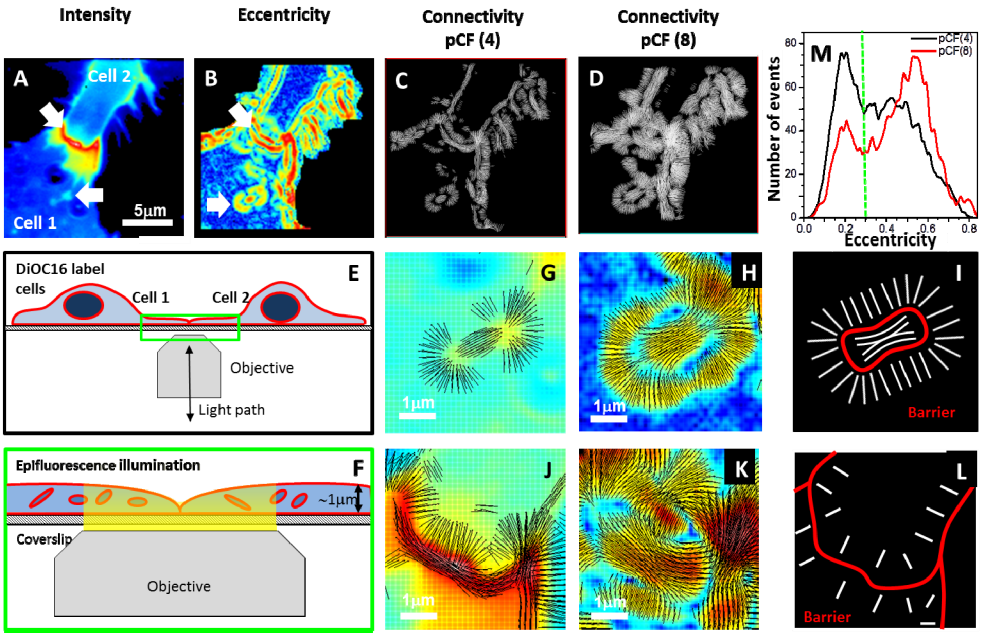

Fig. 7. U2OS cell labeled with DiOC18 imaged with a widefield microscope with epi-fluorescence lamp illumination. A) Intensity image. White arrow indicate an obstacle. B) Eccentricity calculated according to Eq. (6). C) Connectivity map for the pCF calculated at 4 pixel distance (0.456 µm) and D) Connectivity map for the pCF (8 pixels, 0.916 µm). E) Schematic representation of a two cells junction of panel A. F) The cells are very thin at this location so that wide field illumination does not produce much out-of-focus background. G) Zoom of the flow of molecules generated by the structure indicated by the white arrow in panel A and B. Obstacle seen after computing the 2D-pCF at a distance of 4 pixels. H) The same obstacle indicated by the white arrow but after computing the 2D-pCF at a distance of 8 pixels. I) Schematic representation of the expected flow for nearby membrane structures. White lines are representing the connectivity along the membrane structures and the red line represents a barrier. See Fig. 5 for a simulation of molecules moving around or inside a box that show that connectivity lines departing from a surface can be observed if the surface has high curvature. J) At pixel resolution the image shows the diffusion of the dye along the membrane at the junction between the two cells. K) The same junction explored at a longer distance (pCF at 8 pixels). L) Schematic representation of the flow expected at the two cell junction and plasma membrane where red is the barriers and the white lines indicate the connectivity. M) Envelope of histograms of eccentricity for pCF(4) and pCF(8). The vertical line indicates the threshold used for the connectivity maps shown in C and D. For this experiment 10,000 images were collected within a total time of 100 s. The background colors in the zoomed images G,H,J and K are the values of the anisotropy.

The difference in the connectivity maps calculated at a distance of 4 and 8 pixels is notable and it shows that the motion in the membranes is very local. The white arrow in Fig. 7(A) indicates a possible obstacle the dye molecules have to move around. Figures 7(G), 7(H) show that the 2D-pCF can reveal the occurrence of barriers and obstacles. At 4 pixels pCF distance, the two bright spots look connected and at 8 pixels distance the connectivity map strongly supports this hypothesis. Moreover, the comparison between pCF(4) and pCF(8) shows the occurrence of an impenetrable barrier for the dye. These results can be interpreted as the occurrence of a non-lipidic barrier around of a piled up membrane structure. The analysis of Figs. 7(J), 7(K) yield a clear result, supporting diffusion of the dye along the membrane at the cells junction. It is possible to identify that the dye cannot cross this section and this result is more evident comparing the results in pCF(4) vs pCF(8) pixels distances.

Biomedical Optics EXPRESS

5.2 Elucidating obstacles and barrier in vivo of a cell expressing EGFP

Next, we measured EGFP diffusing in cells obtained with the sideSPIM microscope (Fig. 8(A) 8(B)). Figure 8 shows the eccentricity of the diffusion and the connectivity map. In this case we do not have specific expectations about paths the EGFP molecules will follow in their diffusive motions detected by the algorithm for the pCF calculation other than that the pCF should be sensitive to barriers and obstacles for diffusion. By calculating the pCF at different distances we should be able to detect different paths for diffusion. In this case the system is fully three dimensional and we only measured an optical section of the cell.

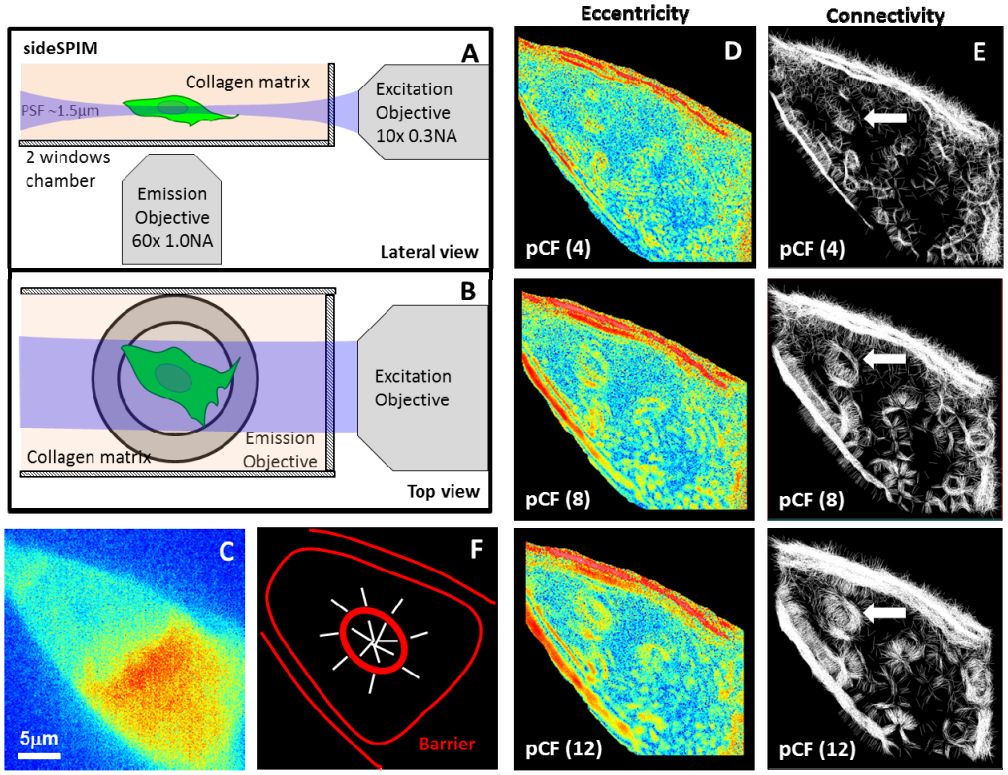

Fig. 8. MB231 cell transfected with EGFP growing in collagen I. Measurements obtained on the sideSPIM microscope at 100 frames/s. Schematic representation of the cell view with respect to the light sheet. A) View from the side. B) View from the top, this view is the image taken by the camera. C) Intensity image. D column) Eccentricity calculated at 4, 8 and 12 pixel distance. E column) Connectivity map for 4, 8, and 12 pixel distance (0.432, 0.864 and 1.296 µm, respectively). The white arrow in E) indicates an obstacle that forces the molecules to go around. F) Expected connectivity pattern for an obstacle of a size of several microns with high curvature and in for the cell membrane.

We note that in the intensity image (Fig. 8(C)) there are no evident objects or barriers. Nevertheless, from the connectivity map (Fig. 8(D)) we can see obvious obstacles for diffusion due to the external cell membrane and due to internal structures that shows up as molecules are going around an object as indicated by the white arrow (Fig. 8(C)). By using longer distances for the computation of the 2D-pCF the occurrence of barriers that restrict the diffusion of the EGFP was evident and at the distance we used for the analysis these barriers were impenetrable (Figs. 8(D), 8(E)). A model for the obstacles highlighted by the white arrow is proposed in Fig. 8(F). This obstacle is located inside the nucleus, which suggests the presence of a nucleolus. Also, in Fig. 9, we show the nucleus contour using a white dotted line obtained from the CMS of the cell. The superposition of the connectivity map on the

Biomedical Optics EXPRESS

CMS image allowed us to highlight the obstacles and barriers inside the cell (Figs. 9(A), 9(B)). In Fig. 9(C) we show schematically that the presence of a barrier to diffusion results in a change of the center of mass of the angular distribution of the pCF function because the distribution is essentially one sided, so that the center of mass is shifted away with respect to the barrier.

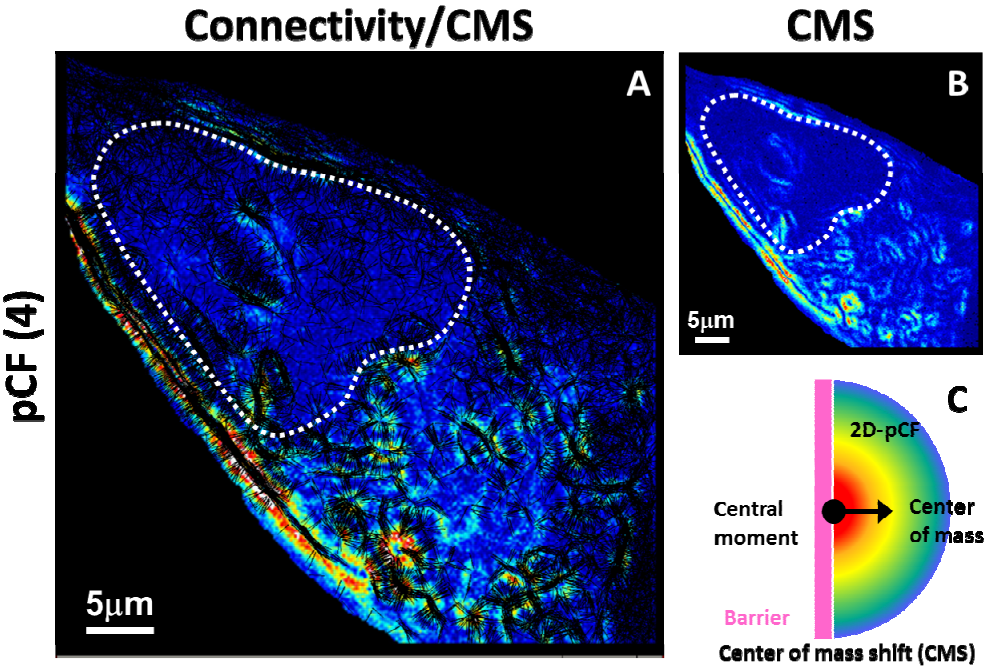

Fig. 9. Connectivity map overlap to the center of mass shift (CMS) image for Fig. 8. A) The connectivity maps (dark lines) were plotted on top of the CMS at pCF(4) in a MB231 cell transfected with EGFP. B) CMS at pCF(4) in a MB231 cell expressing EGFP. C) Schematic representation of the CMS concept. The pink stick represents an impenetrable barrier and the hemi circle represents the 2D-pCF. The CMS is defined as the displacement of the first order moment of the pCF distribution. The displacement of the center of mass of the 2D-pCF distribution will occur in the proximity of a barrier since the cross-correlation between on point in one side of the barrier and another point in the other part of the barrier will be zero.

6. Conclusions

In this paper we describe a method based on the 2D-pCF to produce high resolution maps of molecular movements in cells. We proceeded following three logical steps. First, we presented the 2D-pCF algorithms and discussed the algorithm for construction of the connectivity map using simulations starting from the 2D-pCF. Second, we tested the algorithm in physical systems where EGFP molecules were constrained to move in artificially produced grooves and in the membrane of a GUV. Third, we used cells with a membrane dye and cells expressing the enhanced green fluorescent protein (EGFP) which is known to have minimal interactions with cellular scaffolds and membranes. For a proof of principle, we first collected data of a thin portion of two cells touching each other using a wide field microscope with epi-fluorescence lamp illumination. Finally, we used SPIM microscopy where the spatio-temporal fluorescence fluctuation can be measured at any position in a thick sample due to the optical sectioning capability of this instrument with the required spatial and temporal resolution. In each case we obtained connectivity maps using the algorithm described in the method section showing barriers for diffusion and obstacles that force

Biomedical Optics EXPRESS

molecules to go around. The algorithm to measure the 2D-pCF in an image is the basis for visualizing the spatial connectivity map in the living cell.

For the 2D-pCF approach, we present preliminary simulations to demonstrate the algorithms that we are developing to visualize connectivity maps. There are two notable consequences of the definition we are using for the 2D-pCF: i) it contains the information on the diffusion tensor of the molecule and ii) it is sensitive to displacements smaller than the optical resolution. This is shown in Fig. 2(D) and 2(E) that differ by one pixel in the distance from the barrier. In the simulation the PSF was 300nm. A relevant result of this work is the demonstration that large frame sCMOS cameras for the SPIM microscope can be used as a sensitive detector for molecular fluctuations. While the EMCCD camera has a gain that is uniform and also the noise is uniform across the camera field, the sCMOS camera has a gain (sensitivity) that is different for each pixel. In addition, the noise is not Poissonian and pixels are correlated at a distance (mainly along rows and columns). Therefore, the use of these cameras for spatio-temporal fluctuations is not trivial. We have partially solved the problem by constructing a matrix of gain for each pixel and by avoiding bad pixel. Another way to deal with the noise of the sCMOS camera is to randomize the intensity of two adjacent pixels, which is the method used in this paper. The correction routine is part of the software to calculate the 2D-pair correlation function. For our sCMOS camera we have analyzed the dark noise and we have found that some pixels have a large background. We marked these pixels as bad so that they are not used in the calculations. In addition, the sCMOS camera has correlations between lines, likely due to the process of reading the camera. Before calculation of the 2D-pCF correlation function we perform a local randomization of the points along a line with the adjacent points (simply we exchange the order, but randomly). If this procedure is not applied, some extra correlations (along the lines) are visible only if the intensity is very low. Since the routine is applied if selected, the user can choose not to apply the routine and observe the differences. The ability to use sCMOS cameras for fluctuation spectroscopy is a crucial development for the entire community since these cameras are fast and relatively inexpensive.

One important issue for the application of the 2D-pCF algorithm is that the system must be stationary for the duration of the measurement. For the measurement reported in this manuscript the duration was about 100s. If motion of the cell or part of the cell occurs during the observation time, we could have measurement artifacts. There are general procedures to detect motion artifacts, such as fiduciary markers or motion correction algorithms. Although these methods were not applied to the data shown in this work, we have implemented a "moving average" method in our software based on dividing the total duration in shorter segments and comparing the data for each of the shorter segments. This allows us to detect motion artifact and possibly excluding the segments where the artifacts are present. Based on simulated data, the effect of motion is not detectable if the total drift is less than 1-2 pixels (typically a pixel is about 100 nm) during a data segment. However, if the motion is about 10 pixels or more then the motion appears as an additional eccentricity in the direction of the motion. In this case we disregard the segment or the entire measurement.

A final comment is about comparison with other methods that have been used to map the molecular connectivity in a cell, notable methods based on FLIP-photobleaching [43]. A fundamental difference between fluctuation and photobleaching methods is that fluctuations are measured at equilibrium and on minimally perturbed systems. Fluctuations methods can be used continuously and over an extend period of time in the SPIM microscope, allowing to follow stimulation of events until the stimulus has finished. Fluctuation methods are intrinsically single molecule approaches and in this respect can be compared with single particle tracking. Photobleaching is an ensemble approach and, although very powerful and used by many, it provides average information. This average information could be all you need but we are pointing out here the difference between the 2D-pCF and the bleaching based approaches.

Biomedical Optics EXPRESS

Appendix

Material

The DiOC18(3) (3,3′-Dioctadecyloxacarbocyanine Perchlorate) and all the medium for cell culture were acquired from Molecular Probes-Life Technologies (Thermo Fisher Scientific Inc. Huntington Beach, CA-USA). The 1,2-dioleoyl-phosphatidylcholine (DOPC) was purchased from Avanti Polar Lipids Inc. (Alabaster, Alabama-USA). All chemicals and solvents used were high-grade quality and acquired from Sigma-Aldrich (St. Louis, MO-USA).

GUV preparation

Giant unilamellar vesicles (GUV's) were prepared following the protocol described by Moens at al [42]. Briefly, a dioleylphosphatidycholine (DOPC) was prepared at a final concentration of 0.3 mM in chloroform. DiOC16(3) at 0.5% molar was added to the chlololormic lipid mixture. Then, 4 µL of the organic mixture was applied to the each platinum wire and dried in vacuum overnight. The electroformation chamber was filled with 300 µL of sucrose 200 mM at 50°C, to keep the temperature constant by a circulation bath at 50°C. For the GUV growth, we applied a sinusoidal potential of 2 V and 10 Hz during 1.5 hour. To detach the GUV's from the wire the frequency of the sinusoidal voltage was reduced to 1 Hz for 10 min, and then the function generator and circulating bath were turned off. For the measurements, 50 µL of the GUVs dispersion were transferred to the 2-windows multiwell chamber designed for the sideSPIM imaging containing 300 µL of a 200 mM glucose solution. The GUVs were deposited on top a coated resin with 1 mg/ml bovine serum albumin (BSA) solution. GUV's data acquisition was done at room temperature.

Cell culture

Bone U2OS (ATCC HTB-96) or epithelial MB-231 (ATCC HTB-26) cells were grown at 37°C in 5% CO_2 in Dulbecco's modified Eagle's/F12 (1:1) medium (Gibco, Lifetechologies, Thermo Fisher Scientific Inc. Huntington Beach, CA-USA) supplemented with 10% fetal bovine serum and 5 mL of Pen-Strep. Freshly split cells were plated onto 35-mm MatTek glass-bottom dishes (MatTek Corporation, MA-USA) coated with fibronectin 24 hours before the experiments. Bone U2OS cells were plate in a homebuilt chamber for the sideSPIM imaging. The cells were seeded in a 2 mg/mL collagen type I matrix according to the manufacturer's protocol (BD Bioscience, Bedford, MA-USA). Before imaging the cells were incubated with 1 µM of DiOC18(3) for 30 minutes and then the medium was refreshed. MB-231 cells were stable expressing EGFP.

sideSPIM and TIRF microscopy instrumentation

Fluorescence images were acquired using a home-built sideSPIM setup controlled by Micro-Manager (available at www.micro-manager.org). The sideSPIM was designed on an inverted microscope (IX71 fitted with epifluorescence illumination unit, Olympus) with camera detection sCMOS pco.edge 4.2 (PCO AG, Kelheim-Germany). A motorized MS-2000 xy automated stage (Applied Scientific Instrumentation, OR-USA) holds a piezo xyz-stage (NANO-PDQ375, Mad City Labs) fitted with a custom magnetic sample holder insert. For excitation a white laser source WL-SC-UV-3 was used (Fianium INC, USA), and for EGFP excitation a 480/30 nm ET bandpass filter (Chroma Technology Corporation., Bellows Falls, VT-USA), for DiOC16 excitation a 572/15 nm bandpass filter (Chroma Technology Corporation., Bellows Falls, VT-USA) were needed to select the excitation band. For the EGFP and DiOC16 fluorescence emission a 535/50 nm bandpass and 610 nm longpass filter were used (Chroma Technology Corporation., Bellows Falls, VT-USA), respectively. On the excitation side the objective was a 10XW CFI Plan Fluorite NA 0.3 (Nikon, Japan) and for emission a 60XW LUMPLFLN NA 1.0 water dipping lens (Olympus Corporation, Waltham,

Biomedical Optics EXPRESS

MA-USA) was used. A 10 ms exposure time was used for the 2D-pCF data acquisition. A detailed description can be obtained from [41].

Measurement on widefield instrumentation were done in a commercial Olympus TIRF microscope (Olympus, USA), using mercury lamp illumination and two filter set, for EGFP a HQ500/20 and 515 nm long pass filter split by a Q515lp dichroic mirror (Chroma Technology Corporation., Bellows Falls, VT-USA), for DiOC16 a Texas red D560/40 nm and 610 nm long pass filter split by a 600 nm long pass dichroic mirror (Chroma Technology Corporation., Bellows Falls, VT-USA). The signal was collected using an Olympus TIRF UIS2 PlanApo N 60x (NA = 1.45) oil-immersion objective and fluorescence fluctuation was recorded by an EMCCD camera 512B Cascade (Photometrics, Tucson, AZ, USA). The frame rate was 10 ms and the image size 128x128 pixels.

Optimization and testing of the 2D-pCF algorithm using a simulated experiment

The algorithm to calculate the pCF(δr) (Eq. (1)) as a function of the distance, δr, for each point of an image has been parallelized in order to reduce the computational time and the memory requirements. The algorithm constructs what we call a "sprite' at each point of the image. A "sprite' is a small image of 32x32 points. The first index is the angle and the second index is the delay time in log scale. The sprite image is what is shown in the polar images in Fig. 2 (panels D to I). Given a point, the algorithm calculates a sprite for each distance δr. So for an image of 256x256 pixels there are about 2^{16} sprites, and the calculation is repeated for 4 to 8 distances δr, for example, for each δr we produce a sprite file of about 2^{26} or 256 MB (4 bytes per entry). The sprites, calculated only once, are compressed and stored in the relatively small sprite file. The visualization of the results of the 2D-pCF calculation is done by computing the central moments of each sprite polar image. There are a total of 5 parameters from the central moment's calculation (Center-x, Center-y, ellipses long axis, ellipse short axis and ellipses direction) for each sprite (Eqs (2)-(7)). These 5 primitive maps are used to construct all the derived maps including diffusion eccentricity and anisotropy, time delay long, time delay short, angle, velocity modulus and angle of velocity, and the connectivity map. The calculation of the maps from the sprite file is virtually instantaneous because there is no fit, but only calculation of the second order moments for each sprite map. Also the 5 primitive maps are compressed and stored with a typical size of less than 1 MB total. The highly parallelized calculation of the sprites for a 256x256 image stack of 32,768 frames (about 4 GB of data) takes less than 60 s in a laptop and produces a reduced representation of the diffusion eccentricity and connectivity in files of less than 1 MB. The visualization of connectivity uses the eccentricity and the time delay maps and it does not require re-calculating the sprite file again, since it is a simple visualization of a combination of the maps. For the connectivity map we first establish a threshold value for the eccentricity, for example 0.45. Then at each pixel we plot a segment that has the orientation of the diffusion anisotropy (the ellipses direction) at that pixel and a length proportional to the long axis of the ellipses as shown in Fig. 2. The algorithms for the calculation of the sprites can be found in the program SimFCS available at www.lfd.uci.edu.

Funding

NIH P41-GM103540 and NIH P50-GM076516.

Acknowledgments

This work was initiated by Carmine Di Rienzo during his visit to the Laboratory for Fluorescence Dynamics in 2015-2016. Carmine Di Rienzo tragically passed away in July 2016. We have continued this work and we will like to dedicate this paper to Carmine's memory. We thank Milka Stakic for helping with cell preparations. We thank Emma Mah for providing the groove sample used for Fig. 4. We thank Christoph Gohlke for developing the

Biomedical Optics EXPRESS

fast routines for the calculation of the 2D-pCF sprites method. LM is supported for the Universidad de la República-Uruguay as a full time professor.

Disclosures

None to declare.